JOURNAL OF SOLID STATE CHEMISTRY 31, 113–125 (1980)

Domain and Surface Structures of Sodium Tungsten Bronzes, Na_xWO_3 ($0.4 < x < 1$)*†

MASAO ATOJI

Chemistry Division, Argonne National Laboratory, Argonne, Illinois 60439

Received October 16, 1978; in revised form March 5, 1979

Polarized-light microscopic observations have shown that the birefringent, twin-domain structure of metallic sodium tungsten bronze is exhibited by Na-deficient surface films and hence is not, as had been reported elsewhere, a bulk property. The film can be synthesized by anodic electrolysis in alkaline solution. It is chemically inert, translucent, and often laminates to a multiple layer. The domain structure of the film is hypersensitive to lateral stress and to thermal variation, exhibiting a marked change at the phase transition of the substrate through apparent epitaxial coherence. The domain-wall movement is often slow enough to be visible, and the thermally induced domain modulation is occasionally accompanied by audible high-pitched sound. The bulk structure of the substrate exhibits pseudoperiodic subboundaries that are probably caused by growth defects and the segregation of the sodium atoms. The near-surface of the substrate also shows the sodium segregation that tends to precipitate in periodic patterns. Optical and morphological properties of the substrate structures exhibited no detectable change due to thermal variation or external stress.

1. Introduction

Sodium tungsten bronzes, Na_xWO_3 with $0.45 < x < 1$, are nonstoichiometric, metallic compounds. The bronzes were first prepared by Wöhler (*1*) in 1824. X-Ray structure study of the bronzes was initiated in 1932 by de Jong (*2*), who assigned the bronze structure to the ideal perovskite type based on the cubic sublattice of tungsten and the assumed positions of oxygen and sodium. Until recently, this X-ray structure was refined only on the cubic unit-cell dimension a_0 at various x values as represented by $a_0(\text{Å}) = 0.0819x + 3.7846$ (*3*). The structure comprises a WO_3 matrix, the interstitial Na^+ ions, and an equivalent number of quasi-free conduction electrons as represented by $Na_xWO_3 = xNa^+ + WO_3 + xe^-$. For further details and references, see the review articles (*4–8*).

By polarizing microscopic measurements, Ingold and DeVries (*9*) discovered that the bronze single crystal exhibits birefringent, twin domains at room temperature. The optical characteristics were interpreted in terms of a tetragonal cell with c/a slightly less than one (between 0.990 and 1.000) and twinning on {101}. They also found that the domain walls can be modulated by bending stress and that the tetragonal phase transforms to the cubic structure on cooling and also on heating; for example, at −13 and 146°C for $x = 0.75$. Ingold and DeVries

* Work was performed under the auspices of the Division of Basic Energy Sciences of the Department of Energy. Additional details of this study and a review on the bronze properties are given in M. Atoji, Argonne National Laboratory Report ANL-78-63 (1978).

0022-4596/80/010113-13$02.00/0

attributed all of these observations to bulk properties of Na_xWO_3.

The first neutron diffraction study of the bronzes (*10*) found the following: the structure is not the ideal perovskite type and the atomic parameters (*10*) indicate the oxygen octahedra are tilted alternatively about 4° in the ⟨110⟩ directions; the X-ray unit-cell dimension has to be doubled; the Na atoms are not necessarily all equivalent and can be distributed in two different atomic sites; and the nonperovskite distortion is larger at lower temperatures but no abrupt transition was found at 296–77°K. The neutron reflections showed abnormal peak broadening in some zones, indicating a complex admixing of growth defects and certain twinnings. The peak profile analysis was difficult and hence the overall integrated intensities were employed to obtain an averaged structure. Another neutron study at room temperature has recently been published but it was based solely on powder data (*11*).

More recently, by means of X-ray single-crystal lattice-parameter measurements, Clarke (*12*) found an additional transformation within the tetragonal region, leading to four structure phases which are designated here as Cubic I, Tetragonal I, Tetragonal II, and Cubic II. The transition temperatures are, successively, $T_1 = -8$, $T_2 = 54$, and $T_3 = 147$°C for $x = 0.75$, for example. The tetragonality c/a is about 0.9987 in average. The above symmetry assignments and the proposed structures of Clarke (*12*) have not been confirmed by neutron structure analysis. A Raman scattering study (*13*) also found these four phases using the single crystals obtained from the same batch as Clarke's.

The surface-related properties of the bronzes have been reported in a number of publications. Spitzin and Kaschtanoff (*14*) stated that the bronze powders (1–20 μm) contain up to about 0.4 wt% (6 mole%) of absorbed water which can be removed by heating to 200–300°C. Straumanis and Dravnieks (*15*) reported that when the sintered bronze is exposed to moist air, the electrical resistivity increases with time, due probably to a surface-layer formation on the intergrain boundaries. Consadori and Stella (*16*) observed that the bronze being exposed to air exhibits time-dependent spectra in optical reflectivity, indicative of a film growing on the surface. Based on electrochemical measurements, Vojnović *et al.* (*17*) proposed a structural model of a hydrated layer of nonstoichiometric oxide which is presumably formed on the surface of the bronze in *acidic* solution. This aspect was studied more quantitatively by McHardy and Bockris (*18*) using optical reflectance spectroscopy and ion-probe mass spectroscopy. The bronze surface thus revealed is partly depleted in sodium, typically from 0.7 to 0.25 in x, to the depth of about 500–2000 Å, and exhibits n-type semiconducting characteristics. According to Šepa *et al.* (*19*), the bronze surface in contact with aqueous media hydrates spontaneously. This is followed by some depletion of sodium through an irreversible exchange with hydrogen ions (*20*). The above processes occur more readily in *alkaline* solution. Wertheim *et al.* (*21*) have shown in the X-ray photoelectron spectroscopy that the bronze surface is quickly oxidized by oxygen and water in the atmosphere. The bronze is inert to most chemicals and hence can be an economical substitute for noble metals, particularly as electrodes in electrochemical and catalytic applications ((*17–20*) and the references therein). However, none of these numerous surface-related studies have reported the optical microscopic observation of their bronze specimens.

In conjunction with the neutron study, we have examined various untreated and treated surfaces of the bronzes using polarized-light microscopy. We confirmed most of the Ingold–DeVries observations (*9*) but found some inexplicable aspects. Our

subsequent experiments indicate that the Ingold–DeVries observations were made most likely on Na-deficient, surface films. The explanation of this conclusion is a major subject of this paper.

Another major subject is the characterization of macroscopic inhomogeneities in the bulk structure, since the sample inhomogeneity has caused many controversies in the bronze study. Typically, the electrical resistivity has been measured with successively improved homogeneity, yielding substantially different results: The first measurement in 1954 (*22*) indicated a resistivity minimum implying an ordering of sodium atoms at $x = 0.75$; in 1961 (*23*), the refined experiments found no such minimum and hence no sodium ordering; in 1967 (*24*), an anomaly, although much smaller, was rediscovered near $x = 0.75$. The theoretical interpretation of the electronic transport has similarly been controversial (*25*), chiefly because of the bulk inhomogeneity.

2. Surface Film

a. Characterization and Formation

The birefringent twin structure of the Ingold–DeVries type (*9*) exhibits the characteristics of an epitaxial surface film as follows. First, the twin-structure layer is translucent as evidenced below. Surface blemishes (scratches, pits, and the like) are visible through the twinned layer at both the maximum and minimum contrasts in the birefringence. The twin domain is unperturbed by minor blemishes. The blemishes are situated at a deeper focal plane. The twinned layer was found to be a single film or a lamination of up to several films.

Second, if the twin structure were a bulk property, we should be able to observe a coherent, rational relation among the twins of the orthogonal {100} faces; for example, the *a–a* twin on (010) and the *a–c* twin on both (100) and (001) (*9, 26*). Our search for such a twinning relation has been fruitless in both naturally occurring and strain-free cut crystals. This is also true for the synthetic surface film described below.

Third, and perhaps most important, it was found that the twins of the Ingold–DeVries type can be synthesized on the untwinned surface by electrolytic anodization in alkaline solution. The bronze anode and the noble-metal cathode are placed in 10% NaOH or KOH aqueous solution. The electrolysis is performed at about 0.1–0.2 A/cm^2, 3–9 V (dc) for several seconds while stirring the electrolytic solution vigorously. A similar, but less effective process is to wet the bronze surface with an alkaline solution in the presence of oxygen. The electrolytically synthesized twinned film on the etched surface is shown in Fig. 1. The best crystallized twins can be produced electrolytically on the polished (100) surfaces (Figs. 2 and 3).

In favorable cases, sharp focusing could be made on the surfaces of the outer films and occasionally further down on the surfaces of the inner films and the substrate. The resultant focal-plane differences gave typically about 5–10 μm for the single film thickness and roughly 40 μm for the entire laminated-layer thickness. On the other hand, the film is sometimes too thin to be measurable by optical microscope, meaning the thickness is less than about a micrometer (10^{-3} mm).

In the electrolytic synthesis, when the electrolyte contains insufficient oxygen, the twin domain is formed a few seconds after the electrolytically treated surface is exposed to air. The domain formation is often slow enough to be perceived visually under a polarized-light microscope. The domains can be seen to form at one edge of the surface and migrate to another edge at the propagation speed of about 0.1–1 m/sec. Such a domain-wall migration has also been observed in the thermal and pressure modulation as will be described later.

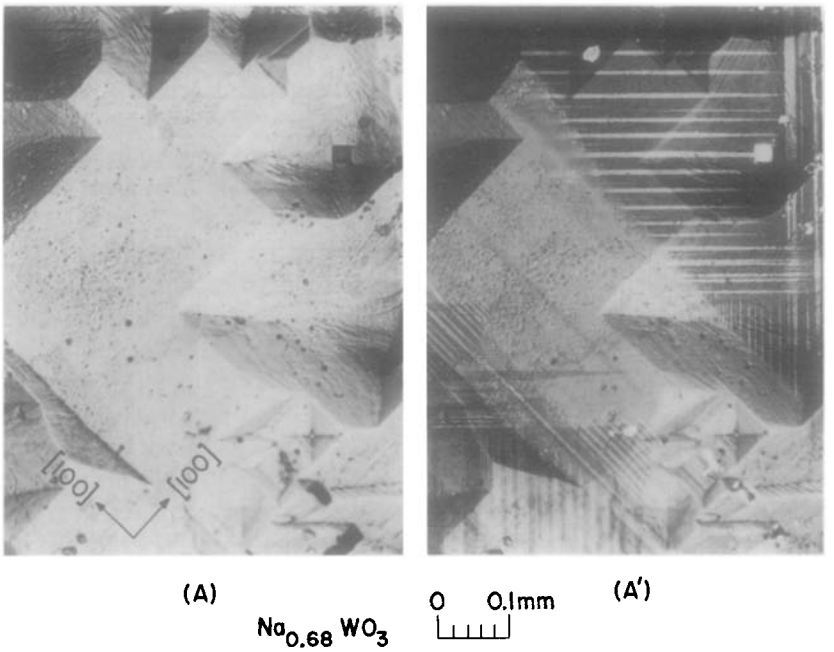

FIG. 1. Polarized-light photomicrographs of deeply etched (010) surface of $Na_{0.68}WO_3$ covered with the surface film. The birefringent contrast is minimum and maximum in (A) and (A'), respectively. In both (A) and (A'), the morphological features of the etched substrate is clearly seen, owing to the translucency of the film. The surface was etched by the modified Murakami reagent and then subjected to anodic electrolysis in 10% NaOH solution for a few seconds at 0.1 mA/cm^2 and 5 V (dc).

The electrolytic synthesis suggests that the twinned surface layer is a hydrated, Na-deficient film (*19*), but not WO_3 or its reduced species. This aspect is in agreement with our X-ray photoelectron and Auger spectroscopic studies. The electrolysis dissolves the substrate continuously, maintaining an equilibrium thickness of the surface film (*19*). However, attempts to isolate the surface film by dissolving the substrate electrolytically were unsuccessful. It appears that the surface film can exist only epitaxially. Electron diffraction in the electrolytically thinned bronze foil indicated that the outer atomic layers of the surface film are considerably dielectric, thereby deflecting away electron beams.

b. Structural Aspects

The twin domains form a variety of multiple stripes as shown in Figs. 1–3. The single-domain width is roughly 0.01–0.001 mm in the orderly narrow stripes and as wide as 0.1 mm in the irregular broad ones. Similar narrow domains have been observed in some ferroelectrics, e.g., $BaTiO_3$ (*26*), Rochelle salt (*26*), WO_3 (*26–31*), etc. As an illustration, we choose the substrate surface to be (010) and assume that the film is strain-free. In Tetragonal I, the median direction of the stripes in the first (innermost) film is parallel to either [101] or [10$\bar{1}$] of the substrate. The stripes in the second film are parallel to either [100] or [001]. The stripes in the third film are the same as the first film, etc. Hence, the angle between the stripes in neighboring film is 45 or 135°, while the stripes within a film can be mutually orthogonal.

At the domain boundary, the optic axis of the domain rotates 90° about the axis perpendicular to the film layer. The angle between the stripes and the optic axis of the

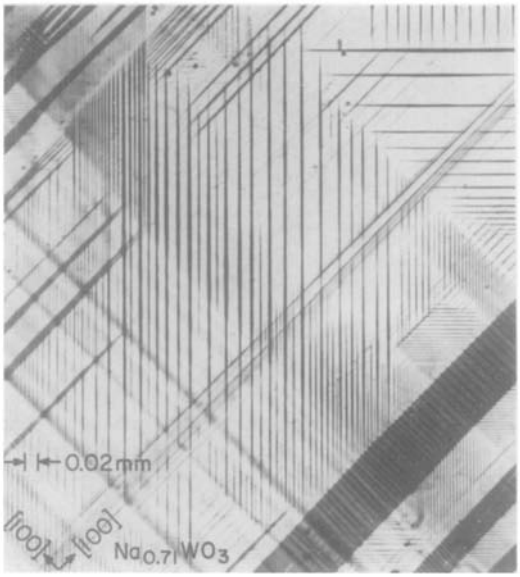

FIG. 2. Polarized-light photomicrograph at the maximum birefringent contrast of the electrolytically synthesized surface films on the polished (010) plane of $Na_{0.71}WO_3$. Some surface blemishes are visible through the films. Several ⟨101⟩ stripes of the innermost film are vaguely seen. The domains of the outer films are seen progressively more distinctively, namely, the ⟨100⟩ stripes of the second innermost film, the ⟨101⟩ stripes of the third film, the ⟨100⟩ stripes of the fourth film, and finally the ⟨110⟩ stripes of the fifth and outermost film. Note that the domain stripes exhibit needle-shaped ends and a bead-loop modulating width.

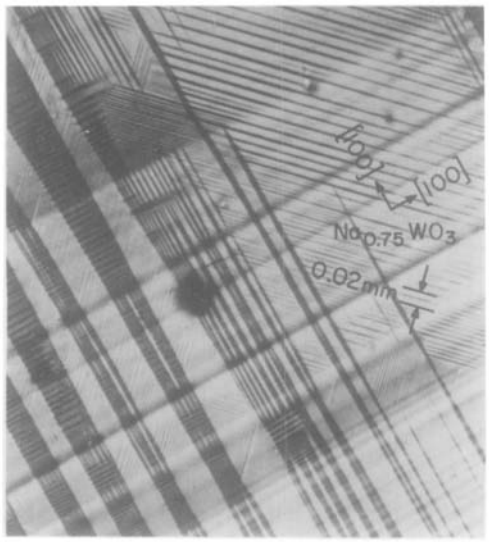

FIG. 3. Polarized-light photomicrographs of the electrolytically synthesized surface films on the polished (010) plane of $Na_{0.75}WO_3$. In addition to the domain characteristics similar to those in Fig. 2, broad twin bands show wedged and fork-like domains.

domain is 45 or 135° in the odd-number films and 0 or 90° in the even-number films. The film structure is probably pseudocubic tetragonal with the layer plane (010) and the optic axis [001]. The twinning plane is then {101} in the odd-number films and (100) or (001) in the even-number films.

As observed in $BaTiO_3$ (*26*), Rochelle salt (*26*), and WO_3 (*27*), the domain boundaries are modulated by any feeble lateral stress, such as a gentle touch with tweezers. As illustrated in Fig. 4, the pressure effect is approximately inversely proportional to the angle between the direction of the applied pressure and the median direction of the domain walls. Hence, at an initial stage of compression, most parallel walls disappear, followed by a gradual decrease of the perpendicular and 45° walls. A single-domain size of 1–0.1 mm in linear dimensions can readily be produced in this manner. When the pressure is removed, the domains reappear and roughly two-thirds of the original pattern is recovered.

The effect of thermal strains is more spectacular as shown in Figs. 5 and 6. The film domain is modulated considerably by such small factors as thermal expansion. Within the phases Tetragonal I and II, the temperature change causes a gradual alteration on the film domain due to the parallel shift of the domain wall. The film domain changes drastically at the phase transition of the substrate. The transition from tetragonal to cubic in the substrate accompanies diminishing of the birefringence of the film. Hence, in the cubic regions of the substrate, the optic axis of the film is perpendicular to the surface or the film structure is cubic. At the Tetragonal I–II transition, the twinning planes undergo rotatory shift of 45 or 135°. Consequently, in Tetragonal II, the stripes in the first film are parallel to [100] or [001] of the substrate,

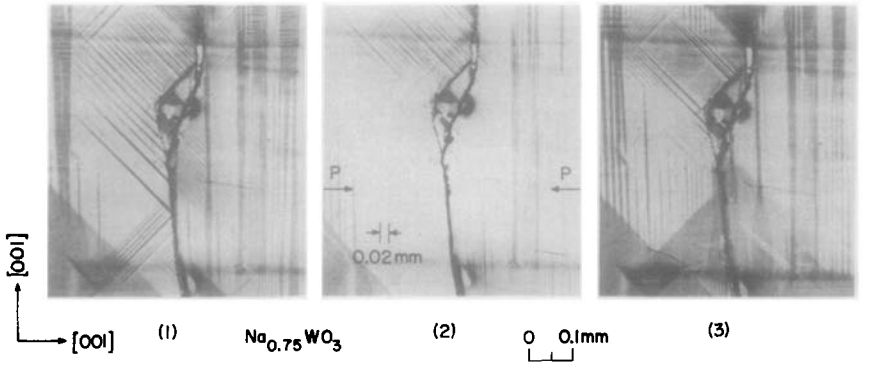

FIG. 4. Polarized-light photomicrographs of $Na_{0.75}WO_3$ showing the effect of external pressure on the domain structure. (1) The original state (zero applied field). (2) The external pressure is being applied parallel to the [001] axis. Most domain walls are diminished. (3) The pressure is released and the original structure is mostly reproduced. The surface under pressure is being deformed cylindrically. The cylindrical axis lies underneath and parallel to the surface and is perpendicular to the pressure.

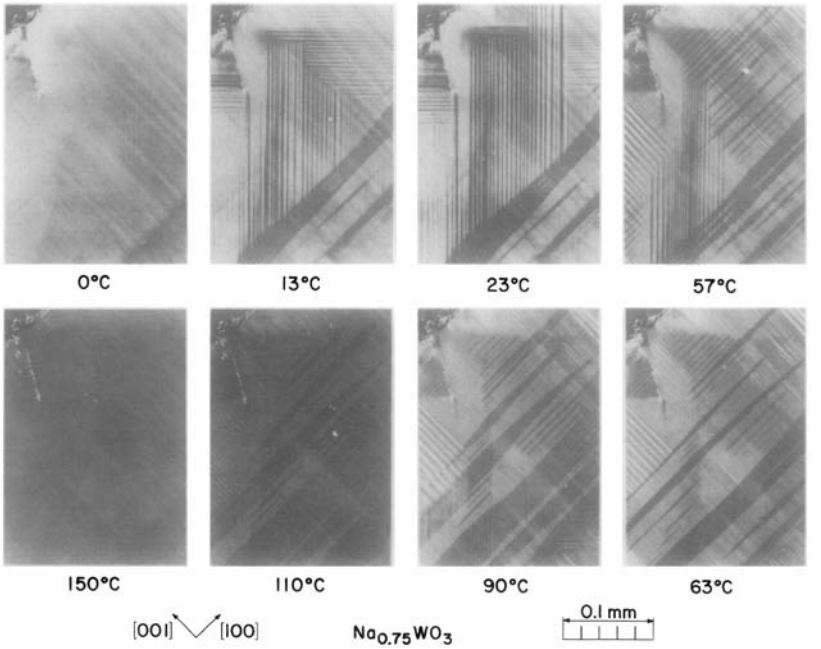

FIG. 5. Polarized-light photomicrographs showing the temperature dependency of the domain structure of the surface film of $Na_{0.70}WO_3$ at 0–150°C. The film domain appears to monitor the phase transitions of the substrate at $T_1 = 9$, $T_2 = 52$, and $T_3 = 148$°C (*12*). At 0°C, the film structure is nearly isotropic or the optic axis of the film is perpendicular to the surface (the substrate is Cubic I); at 13°C, the ⟨101⟩ domains dominate (Tetragonal I); at 23°C, the population change occurs among the [101] and [10$\bar{1}$] domains (Tetragonal I); at 57°C the ⟨100⟩ domains start to appear (the transient state between Tetragonals I and II); at 63°C, the ⟨100⟩ domains dominate (Tetragonal II); at 90°C, the population change takes place among the [100] and [001] domains (Tetragonal II); at 110°C, a further population change occurs among the [100] and [001] domains (Tetragonal II); and at 150°C, the film becomes isotropic or the optic axis of the film becomes perpendicular to the surface (Cubic II).

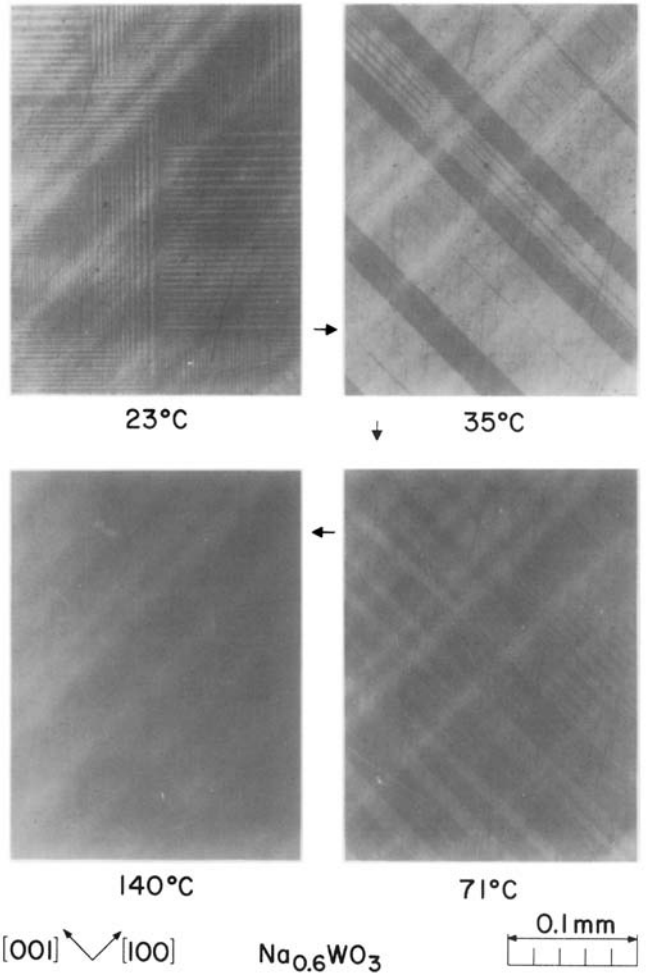

FIG. 6. Polarized-light photomicrographs showing the temperature effect on the surface film of $Na_{0.6}WO_3$ at 23–140°C. The transition temperatures of $Na_{0.6}WO_3$ are $T_1 = 13$, $T_2 = 30$, and $T_3 = 133°C$ (*12*). The domain of the surface film changes in an apparent coherence with the structural change of the substrate. The ⟨101⟩ domains at 23°C (the substrate being Tetragonal I) are replaced by the ⟨100⟩ domains at 35°C (Tetragonal II). The thermoelastic effect changes the optical reflectivity but not the domain configuration as shown by the 71°C pattern (Tetragonal II). At 140°C, the film becomes isotropic or the optic axis of the film becomes perpendicular to the surface (Cubic I).

those in the second film are parallel to [101] or $[10\bar{1}]$, and so on. The thermally induced domain modulation is occasionally accompanied by an audible, high-pitched, snapping sound.

c. Properties

The surface film is chemically more inert than a bulk crystal. The domain structure was uninfluenced by hot concentrated solutions of HCl, HNO_3, HF, H_2O_2, and various admixtures thereof. Concentrated H_2SO_4 modulated the domain structure somewhat due to a dehydration of the film. The surface film, unlike WO_3, is inert to boiling solutions of NaOH, KOH, NH_4OH, Na_2O_2, H_2O_2, and their admixtures. Similar inertness was shown against reducing reagents such as

sodium sulfite and hydroxylamine hydrochloride. The film is also unaffected by anodic and cathodic electrolyses in acids and by cathodic electrolysis in alkaline solutions. Probably the only way to remove the surface film from the substrate is by mechanical polishing.

The effect of hydration in the film is as follows. The domain pattern of the wet film appears fuzzy, but becomes sharply defined when the film is dried at about 60°C. This means that some water molecules are so loosely bound to the film that they can be driven off at about 60°C. The reproducibility of the domain pattern in the thermal cycle is higher for the higher drying temperature. For example, when the film is dried at 60 and 300°C, the reproducibility is about 75 and 95%, respectively. The dry film absorbs the water molecules readily, making the domain pattern fuzzy. When the film is heated above 350°C, oxidation becomes appreciable. Above 400°C, the surface is covered with a blue metallic-luster film of WO_3. In all cases mentioned above, the sample was heated in air for about 1 min.

The bronze single crystals exhibit cleavage parallel to the {100} planes. This cleavage may be not necessarily an intrinsic bulk property, but can be caused by growth defects as described in Sect. 3. Also, the planar crevices can be developed at growth defects, providing readily cleavable planes. In the preparation of the bronze crystal, the excess sodium tungstate in the final product is leached off in boiling water of hot NaOH solution. The sodium tungstate solution is alkaline and hence the leaching process tends to create a sodium-deficient layer not only on the outer surface but also on the crevices. In fact, we have often observed that the freshly cleaved surface in air shows no domain initially but exhibits domain formation a few seconds later.

A pair of opposite faces obtained by cleaving a (010) plane are shown in Fig. 7. The film domains of an as-cleaved pair, A_1–A_1', were not well crystallized. The anodic

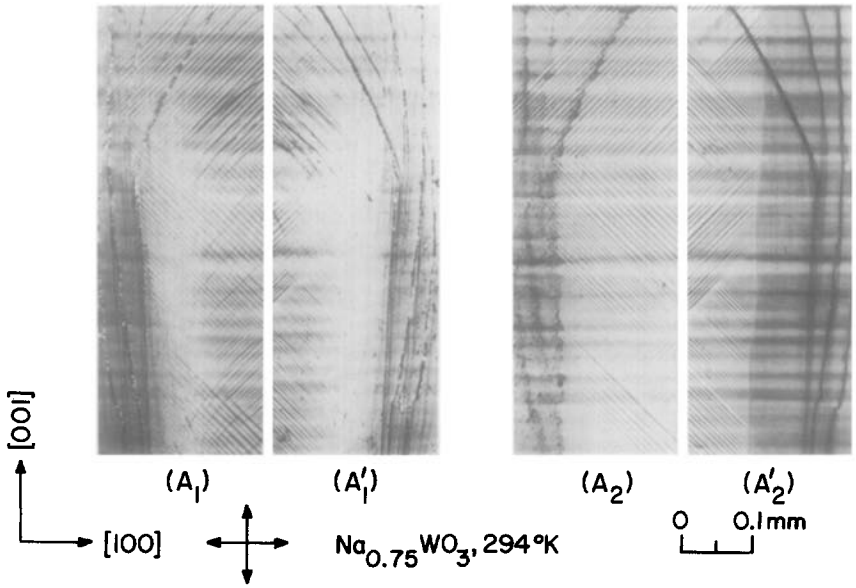

FIG. 7. Polarized-light photomicrographs of a pair of opposite faces obtained by cleaving a (010) plane of $Na_{0.75}WO_3$. The as-cleaved (010) faces are shown in A_1 and A_1'. The same pair after being treated electrolytically are displayed in A_2 and A_2'. The crossed arrows indicate the directions of the polarization vectors of the polarizing and analyzing Nicols. The film domains on these cleavage surfaces suggest that the cleavage is due to a growth imperfection and is not an intrinsic bulk property.

electrolysis in 10% NaOH solution purified and recrystallized the film as indicated by the well-defined domain patterns in the A_2–A_2' pair. In both cases, roughly 60–75% of the domain patterns of the matched pair are identical. The cohesive stacking is realized between the film with the ⟨100⟩ domains and the film with the ⟨110⟩ domains. However, the domains of the outermost film of A_1 and those of A_1' are the same ⟨110⟩ types, resulting in repulsion between A_1 and A_1', hence the cleavage.

The electrical conductivity of the bulk crystal is not appreciably influenced by the formation of the surface film. This resembles Al_2O_3 on aluminum metal, exhibiting a tunneling effect in the electric conduction.

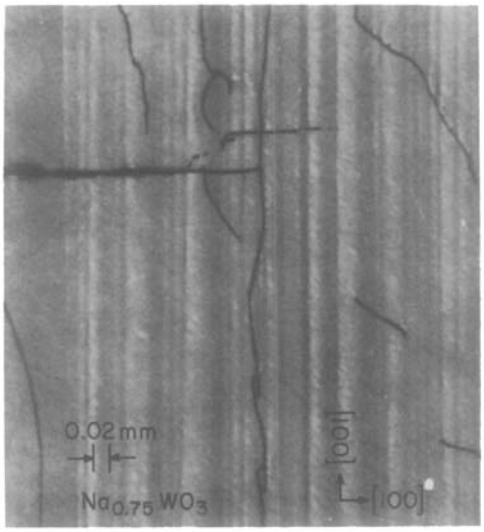

FIG. 8. Unpolarized-light photomicrograph showing a linear segregation of the sodium atoms on the mechanically polished (010) surface of $Na_{0.75}WO_3$. Dark and light regions represent reddish and orange colors, respectively. The sodium content in the former is about 5 atom% less than that in the latter. Weak optical birefringence due to lattice strains is observed along part of the light band adjacent to the dark striation. The polishing was carried out using 0.25 μm diamond paste or water slurry of 0.3–0.5 μm Al_2O_3 powder. A standard double-circle grinder-polisher was employed.

3. Substrate

During the preparation of the metallographic specimen, we noticed that some regions of the mechanically polished surface of the high-x bronze ($x > 0.7$, orange to yellow color) were tinted a brick-red color (darker in a black and white photograph). The red tinting implies a segregational depletion of sodium has taken place during the mechanical polishing. The X-ray microprobe analysis indicated that the sodium content in the red-tinted area is about 5 atom% less than that in the orange-yellow area. The color contrast is most effectively observed with unpolarized light and can be seen with or without the surface film. The color change is less noticeable in the lower-x bronzes.

The shape of the tinted area due to the segregation of the sodium atoms varies from irregular to remarkably regular. Exemplary regular forms of the segregation are linear, rectangular, and crosshatched striations as shown in Figs. 8, 9, and 10, respectively. The directions of these striations are always parallel to the ⟨100⟩ axes. The crosshatched pattern (Fig. 10) can also be produced by

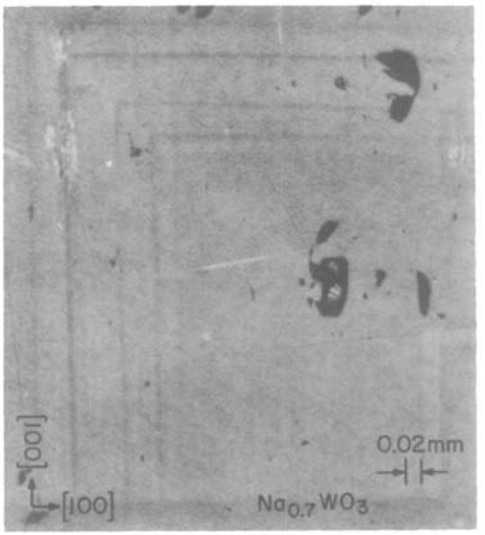

FIG. 9. Unpolarized-light photomicrograph showing a rectangularly striating segregation of the sodium atoms on the mechanically polished (010) surface of $Na_{0.7}WO_3$. Other particulars are the same as in Fig. 8.

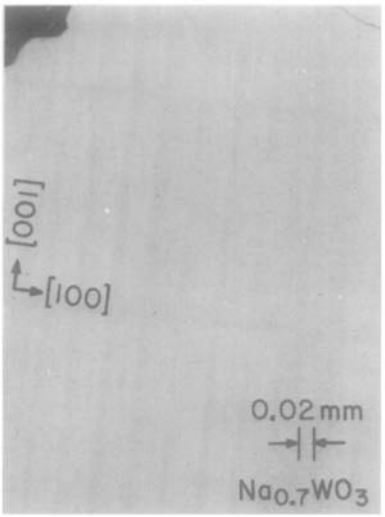

FIG. 10. Unpolarized-light photomicrograph showing a crosshatched segregation of the sodium atoms on the mechanically polished (010) surface of $Na_{0.7}WO_3$. Other details are the same as in Fig. 8, except that the sample was polished using an automatic vibratory polishing machine.

anodic electrolysis of the polished {100} surface in a diluted H_2O_2 solution.

A given surface exhibits different types of the sodium segregation, depending on the surface treatment. Apparently, the lesser strain induced by polishing result in higher ordering in the segregation. A vibratory polishing (*32*) causing the least strain yields the most regular pattern (Fig. 10). Moreover, the sodium segregation on the surface is entirely different from the etch pattern of the same surface. Hence, the sodium segregation mentioned above takes place on the outermost layer of the unetched flat surface and is unrelated to the mechanical twinning. The diffusive migration of the sodium atoms hardly occur in the bulk structure (*33*), but may take place quite readily on the surface. The sodium segregation is seen preferentially in the vicinity of surface blemishes. Conversely, the blemishes or the macrodefects tend to develop along the segregation boundaries.

In order to reveal the substrate structure of the bronze, we have tested exhaustively numerous potentially usable etchants (*9, 34–37*). We found only one suitable etchant, an oxygen-free solution of 10–20% KOH (or NaOH) and 10–20% $K_3Fe(CN)_6$ (*34*). This etchant may be termed a modified Murakami reagent (*37*). The presence of oxygen induces the formation of the surface film on the etched surface. The rate of the etching reaction is faster for higher x (*35*).

When the polished surface was etched slightly using the modified Murakami reagent, the treated surface showed a variety of etch patterns. Examples of the random and regular etch patterns are shown in Figs. 11 and 12, respectively. These observations imply that the sodium atoms near the surface also tend to segregate in striations parallel to the ⟨100⟩ axes.

The deeply etched surface frequently exhibits periodic subboundaries having a pseudodomain appearance (Figs. 11 and 12). The subboundary lines are usually parallel to the ⟨100⟩ axes. Such pseudodomain structures are produced during the crystal growth.

FIG. 11. Unpolarized-light photomicrograph of slightly etched (010) surface of $Na_{0.75}WO_3$, showing the sodium segregation in a venetian-blind pattern. The sodium content is higher in the lighter area. The striations are parallel to the ⟨100⟩ axes. This surface showed no optical birefringence. The surface was mechanically polished and then etched using the modified Murakami reagent at room temperature.

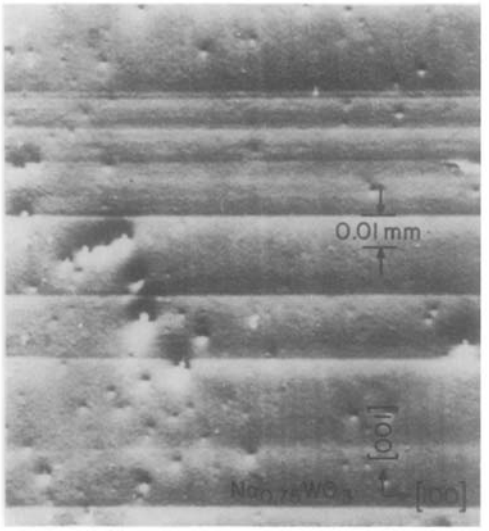

FIG. 12. Nomarski interference-contrast photomicrograph of the (010) surface of the etched $Na_{0.75}WO_3$, showing a pseudoperiodic segregation of the sodium atoms. The parallel subboundary lines are slightly protruded. The diffusely bright bands adjacent to the striations show weak birefringence, which is probably induced by lattice strains. The etch pits could be end-on images of dislocations. Etching was performed using the modified Murakami reagent at room temperature for about 10 sec.

The crystal synthesis undergoes several transient reactions (*38*) and is regulated through the intercorrelation among supersaturation, nucleation, and diffusion, each of which has different temperature and potential dependencies. Nonequilibrium instabilities and inhomogeneities in the temperature, electric potential, and reactant distributions can generate periodic variations in the sodium segregation, the impurity precipitation, and the like. These growth defects occur preferentially in sectors parallel to {100}, inducing readily cleavable planes (see Sect. 2c).

The deeply etched surface of the homogeneous substrate is shown in Figs. 13A and B. The etched figures on the {100} planes are characterized by a square pyramid having either O_h–$m3m$ or T_h–$m3$ symmetry. The T_h symmetry is not necessarily intrinsic and may be attributed to the growth anisotropy. We have never observed the morphological symmetries of other cubic symmetries, T_d–$43m$, O–43. and T–23.

The {110} and {111} surfaces were also studied rather extensively. The electrolytic treatment and the etching processes yield neither well-crystallized surface film nor clearly definable morphological features.

Concerning the optical properties of the substrate, in the pseudodomain pattern (Fig. 12), weak optical birefringence was observed in some portions of the striation lines. The optic axis is parallel to the striation, and the optical extinction varies from vague to somewhat distinct. The extinction axis lies 45° from the ⟨100⟩ axes. Some striations are nonbirefringent, but become birefringent by treating with HNO_3 and HCl. This birefringence is probably due to the local lattice strains and to the sodium segregation.

In addition to the strain-induced optical effect, the surface, the near-surface, and the deeply etched surface of the substrate show no significant birefringence and no change in the optical and morphological properties at the phase transitions (*12*). Similarly, the external stress on the substrate induced no measurable effect. Accordingly, the optical microscopy was unable to establish whether the modulation of the film domain is independent of, or dependent on, the structural change of the substrate.

Acknowledgments

I wish to express my sincere appreciation to the following colleagues: G. T. Chubb for the scanning electron microscopy; G. C. Danielson and R. C. DeVries for supplying some bronze specimens used for the early stage of this study; L. H. Fuchs and R. H. Lee for assistance in the metallographic and optical procedures; C. E. Johnson and C. Seils for the X-ray microprobe analysis; S. A. Johnson for the use of the microscope attachments; M. S. Kaminsky for the Auguer spectroscopic analysis; D. W. Lynch for useful information; P. Okamoto and T. H. Tahmisian for electron diffraction trials; S. Susman for valuable discussions on optics; and R. J. Thorn for collaborating in the X-ray photoelectron spectroscopy.

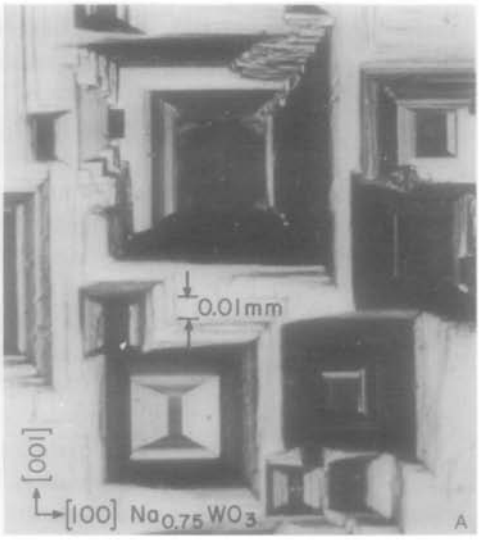

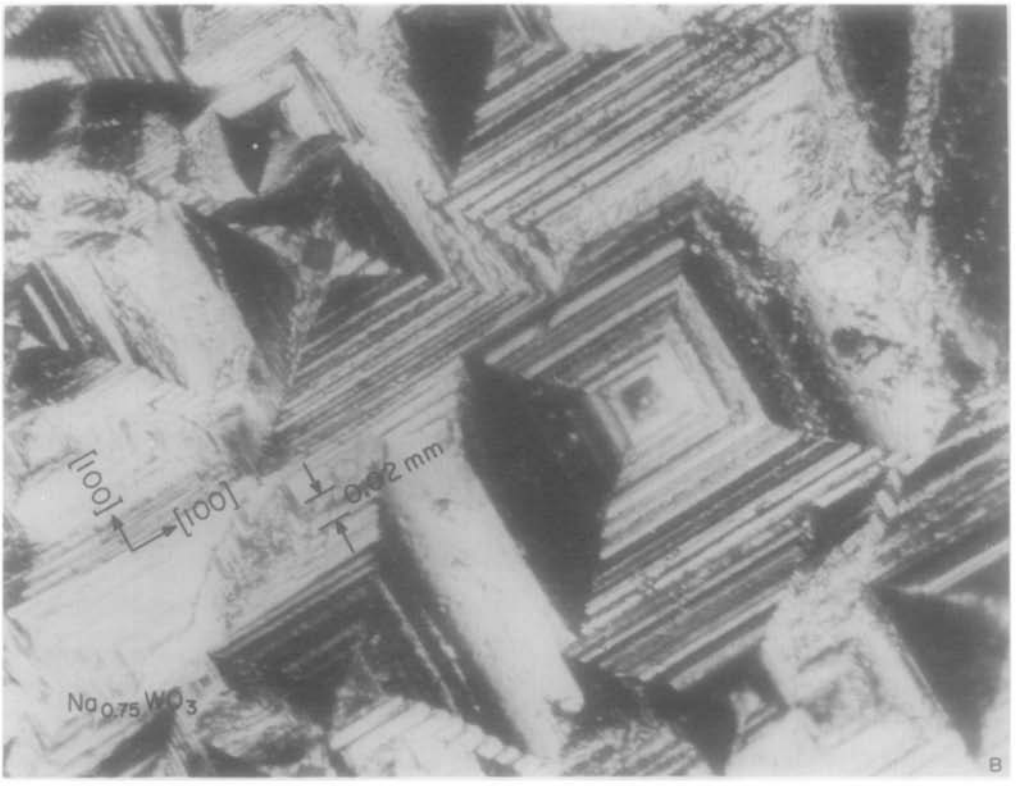

Fig. 13. (A and B) Nomarski interference-contrast photomicrographs of deeply etched (010) surfaces of $Na_{0.75}WO_3$ crystals. The etched figures show morphological symmetries, O_h–$m3m$ and T_h–$m3$. In (B) some pyramid figures have stepping striations which are always parallel to ⟨100⟩. No optical birefringence was exhibited by these patterns. Etching was carried out using a boiling solution of 20% $K_3Fe(CN)_6$ and 20% NaOH for about 10 sec.

References

1. F. WÖHLER, *Ann. Phys. (Leipzig)* **2**, 350 (1824).
2. W. F. DE JONG, *Z. Kristallogr.* **81**, 314 (1932).
3. B. W. BROWN AND E. BANKS, *J. Amer. Chem. Soc.* **76**, 963 (1954).
4. M. J. SIENKO, *Advan. Chem. Ser.* **39**, 224 (1963).
5. H. R. SHANKS, P. H. SIDLES, AND G. C. DANIELSON, *Advan. Chem. Ser.* **39**, 237 (1963).
6. P. G. DICKENS AND M. S. WHITTINGHAM, *Quart. Rev. Chem. Soc.* **22**, 30 (1968).
7. P. HAGENMULLER, *in* "Progress in Solid State Chemistry" (H. Reiss, Ed.), Vol. 5, Chap. 3, Pergamon, Oxford (1971).
8. F. R. GAMBLE AND T. H. GEBALLE, *in* "Treatise on Solid State Chemistry," Vol. 3: "Crystalline and Noncrystalline Solids" (N. B. Hannay, Ed.), Chap. 2, Plenum, New York (1976).
9. J. H. INGOLD AND R. C. DEVRIES, *Acta Met.* **6**, 736 (1958).
10. M. ATOJI AND R. E. RUNDLE, *J. Chem. Phys.* **32**, 627 (1960).
11. P. J. WISEMAN AND P. G. DICKENS, *J. Solid State. Chem.* **17**, 91 (1976).
12. R. CLARKE, *Phys. Rev. Lett.* **39**, 1550 (1977).
13. E. J. FLYNN, S. A. SOLIN, AND H. R. SHANKS, *Solid State Commun.* **25**, 743 (1978).
14. V. SPITZIN AND L. KASCHTANOFF, *Z. Anal. Chem.* **75**, 440 (1928).
15. M. E. STRAUMANIS AND A. DRAVNIEKS, *J. Amer. Chem. Soc.* **71**, 683 (1949).
16. F. CONSADORI AND A. STELLA, *Lett. Nuovo Cimento* **3**, 600 (1970).
17. M. V. VOJNOVIĆ, D. B. ŠEPA, AND D. S. OVCIN, *Croat. Chem. Acta* **44**, 89 (1972).
18. J. MCHARDY AND J. O'M. BOCKRIS, *J. Electrochem. Soc.* **120**, 53 (1973).
19. D. B. ŠEPA, M. V. VOJNOVIĆ, D. S. OVCIN, AND N. D. PAVLOVIC, *Electroanal. Chem. Interfacial Electrochem.* **51**, 99 (1974).
20. J. VONDRAK AND J. BALEJ, *Electrochim. Acta* **20**, 283 (1975).
21. G. K. WERTHEIM, M. CAMPAGNA, J.-N. CHAZALVIEL, AND H. R. SHANKS, *Chem. Phys. Lett.* **44**, 50 (1976).
22. W. R. GARDNER AND G. C. DANIELSON, *Phys. Rev.* **93**, 46 (1954).
23. L. D. ELLERBECK, H. R. SHANKS, P. H. SIDLES, AND G. C. DANIELSON, *J. Chem. Phys.* **35**, 298 (1961).
24. L. D. MUHLESTEIN AND G. C. DANIELSON, *Phys. Rev.* **160**, 562 (1967).
25. B. R. WEINBERGER, *Phys. Rev. B* **17**, 566 (1978), and the references therein.
26. F. JONA AND G. SHIRANE, "Ferroelectric Crystals," Pergamon, Oxford (1962).
27. R. UEDA AND T. ISHINOKAWA, *J. Phys. Soc. Japan* **6**, 122 (1951).
28. T. NAKAMURA, *J. Phys. Soc. Japan* **11**, 467 (1956).
29. S. TANISAKI, *J. Phys. Soc. Japan* **14**, 970 (1959).
30. J. SPYRIDELIS, P. DELAVIGNETTE, AND S. AMLINCKX, *Mater. Res. Bull.* **2**, 615 (1967).
31. S. AMELINCKY AND J. VAN LANDUYT, "The Chemistry of Extended Defects in Nonmetallic Solids" (L. Eyring and M. O'Keefe, Eds.), p. 295, North-Holland, Amsterdam (1970).
32. L. E. SANUELS, "Metallographic Polishing by Mechanical Methods," 2nd ed., Pitman, Melbourne (1971).
33. J. F. SMITH AND G. C. DANIELSON, *J. Chem. Phys.* **22**, 266 (1954).
34. J. PHILIPP AND P. SCHWEBEL, *Chem. Ber.* **12**, 2234 (1879).
35. A. MAGNÉLI, *Ark. Kemi* **1**, 273 (1949).
36. M. E. STRAUMANIS, *J. Amer. Chem. Soc.* **71**, 679 (1949).
37. G. L. KEHL, "The Principles of Metallographic Laboratory Practice," 3rd ed., McGraw-Hill, New York (1949).
38. J. P. RANDIN, *Electrochim. Acta* **19**, 745 (1974), and the references therein.